Iranian Journal of Geophysics, 2019, Page 68 - 81

Seismic Amplification of Peak Ground Acceleration, Velocity, and Displacement by Two-Dimensional Hills

Abdollah Sohrabi-Bidar[1*], Masoud Amel-Sakhi[2], Arash Shareghi[3], and Shahram Maghami[4]

[1]*Associate Professor, School of Geology, College of the Sciences, University of Tehran, Tehran, Iran*
[2]*Assistant Professor, Department of Civil Engineering, Qom University of Technology, Qom, Iran*
[3]*M. Sc. Graduated, Department of Civil Engineering, University of Urmia, Urmia, Iran*
[4]*Ph. D. student, School of Geology, College of the Sciences, University of Tehran, Tehran, Iran*

(Received: 27 August 2018, Accepted: 05 May 2019)

Abstract

There are valuable investigations on the amplification effects of the topography on the seismic response in the frequency domain; however, a question is that how one can estimate the amplification of time domain peak ground acceleration (PGA), peak ground velocity (PGV), and peak ground displacement (PGD) over the topographic structures. In this study, the numerical approach has been used for the evaluation of time domain peak ground motion parameters amplification on a two-dimensional Gaussian-shaped hill in a typical rocky medium. Five normalized geometries, as well as the twelve normalized vertical incident motions, have been used. Incident motions are SV wave of Ricker type. Time domain responses of displacements, velocities, and accelerations have been calculated and analyzed in selected points of the hills. Tabulated results illustrate a significant role of geometry on the patterns of the amplification, and that almost the top of the hill amplifies and the hill toe de-amplifies the motion. Meanwhile, the rate of the amplification and de-amplification generally depends on the predominant period of the incident motion. Comparison of the amplification of PGA, PGV, and PGD values with the Fourier amplification curves showed that, in general, there is a well-matched correlation between them; however, the time domain amplifications of PGA, PGV, and PGD values have a gentler variation with the predominant period of the motion. It seems that one can give a reliable estimation of time domain amplification of PGA, PGV, and PGD values by using averaged Fourier amplifications over the suitable range of frequencies around the predominant period of the input motion.

Keywords: topographic effect, peak ground motion parameters, amplification, two-dimensional hills

[*]Corresponding author: asohrabi@ut.ac.ir

1 Introduction

The effects of surface topography on seismic response have been observed during several earthquakes. Celebi (1987 and 1991) presented some cases of observation of topography effects on the surface seismic response during the 1987 Superstition hill earthquake, 1983 Coalinga earthquake and 1985 Chile earthquake. Athanasopoulos et al. (1999) and Bouckovalas and Kouretzis (2001) have shown evidences of amplification of the site response due to the topography variation during the 1999 Greece earthquake. Wang et al. (2016) studied the earthquake-damaged distributions and its relationship with the local topography during the 2015 Gorkha earthquake in Nepal. Along with this observations, high accelerations recorded in Pacoima dam during 1971 San Fernando Earthquake (Boore, 1973; Trifunac and Hudson 1971) and in Tarzana Hill (1.78g) during 1994 Northridge earthquake (Spudich et al., 1996) are among the cases that refer to the topography as an important factor in site seismic response.

Considering numerical estimation of the topography effects on ground motion, Boore (1972) was the first who used the finite difference method to evaluate the triangle shaped hill induced by SH waves. Then, Bouchon (1973) studied the semi-sine shaped hill in different shape ratios (ratio of hill height to the half width), by scattering SH waves. Later, Bard (1982) studied the scattering and propagation of the P and SV waves by surface irregularities. Besides, Sánchez-Sesma and Campillo (1991 and 1993) studied seismic behavior of semi-elliptical and triangular shaped hill under propagating of the P and SV waves by using the boundary element method in the frequency domain. Further, Ashford et al. (1997) performed a frequency-domain parametric study using generalized consistent transmitting boundaries to evaluate the seismic response of steep slopes. They were able to distinguish between the amplification caused by topography and the one caused by the natural frequency that was advantageous to the development of a simplified method to estimate topographic effects. Zhang et al. (1998) used a hybrid discrete wave-number boundary element and finite element method to study the scattering of SV waves by the trapezoidal shaped hills. Bouckovalas and Papadimitriou (2005) conducted numerical analyses for the seismic response of step-like ground slopes in the uniform visco-elastic soil, under vertically propagating of SV waves. Kamalian et al. (2003 and 2006) developed a hybrid time domain boundary element / finite element method for seismic analyses and conducted an extensive study on two-dimensional semi-sine, semi-elliptical and trapezoidal shaped hill, under vertically propagating P and SV waves. Additionally, Kamalian et al. (2008) studied different parameters such as incident wavelength, shape ratio, Poisson's ratio, and hill shape on ground amplifications under vertically propagating of SV wave. And recently, Sohrabi-Bidar et al. (2009a, 2009b, and 2010) conducted a few parametric studies to demonstrate the three-dimensionality effects of the response of the simple topographic features.

Most of the above-mentioned studies have been performed in the frequency domain. Among the recent works that have been performed in the time domain, the main part of the results has been considered in the frequency domain as well, e.g. conventional amplification spectra.

In most of the previous works, time domain amplification parameters have rarely been considered. While the maximum value of ground motion parameters in the time domain, namely peak ground acceleration (PGA), peak ground velocity (PGV), and peak ground

displacement (PGD), are taken into account as the crucial criteria applied in quite a few design codes and practical purposes. Generally, three ranges of structural periods are likely to be determined within which the values of ground motion acceleration, velocity, or displacement are of the utmost importance. Short-period, moderately long-period, and exceptionally long-period structures typically categorized within the ranges of less than 0.5, 0.5 to ~2, and longer than 2-3 seconds, respectively, which are sensitive to PGA, PGV, and PGD in the order mentioned. The most frequently used parameter is the PGA, which is a traditional and immediate representative of induced seismic forces. Reference PGA on rock site is the main parameter, which is used in many structural codes to describe the seismic hazard level (Solomos et al., 2008). The dependence of intermediate period structures on velocity is directly recognized by the Japanese code 2004 (BSL, 2004), in which the PGV is used for the design of tall buildings.

This study considers and discusses the amplification of the peak ground motion parameters in the time domain induced by simple topographic structures. For this purpose, the numerical approach has been adopted and the seismic response of Gaussian-shaped hills against vertically propagating SV waves of Ricker type has been calculated. Different geometrical dimensions, as well as different dominant frequency of incident waves, have been considered. The tabulated result has been presented and compared to the conventional amplification curves of topographic structures.

2 Numerical Method and Verification

In geotechnical engineering, different numerical modeling methods have been developed and are available for the study of seismic analyses. These are generally divided into two classes, Boundary methods (i.e. Boundary Element Method) and Domain Methods (i.e. Finite Element Method, Finite Difference Method, …). In this study, numerical modelings are performed by using the Finite Difference Method (FDM) and the FLAC code.

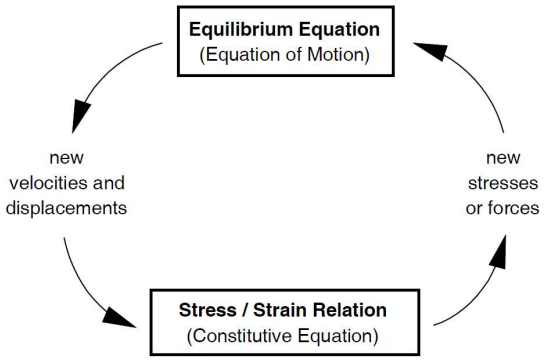

Figure 1. Basic explicit calculation cycle of FLAC (Itasca, 2017).

In FDM, each derivative in the set of governing equations is directly considered by the finite difference approximation of field variables in discrete points of space. The general calculation sequence used in the FLAC is shown in Figure 1. At first, the accelerations and velocities are derived by using the stresses and forces. After that, strain rates are calculated from velocities and new stresses from strain rates. Every cycle around the loop takes one time step and at each time the incremental displacements are added to the coordinates so that the grid moves and deforms with the constitutive formulation of the material it represents. The solution of the problem needs two types of equilibrium and constitutive equations. For dynamic analyses in a continuous solid body, the equilibrium equation is as follows:

$$\frac{\partial \sigma_{ij}}{\partial x_j} + b_i = \rho \frac{\partial^2 u_i}{\partial t^2} \quad (1)$$

where ρ is the mass density, t is the time, x_i is the coordinate vector, b_i is the body force vector and σ_{ij} is the stress tensor for isotropic elasticity material the

constitutive equation which relates stresses to the strain of the body is as follows (Itasca, 2017):

$$\sigma_{ij} := \sigma_{ij} + \left\{\delta_{ij}\left(K - \frac{2}{3}G\right)\dot{e}_{kk} + 2\,G\,\dot{e}_{ij}\right\}\Delta t \qquad (2)$$

where δ_{ij} is the Kronecker delta; Δt is the time step; $\dot{e}_{ij}$ are the components of the rate of strain and G and K are the shear and bulk modulus of the medium, respectively.

In seismic analyses with domain method, the model size and artificial wave reflections from the boundaries are important issue. Based on the Bouckovalas and Papadimitriou (2005) suggestion in seismic analyses with FLAC, model sizes have been set eight times the half-width of the topographic features where at the distance points, the topographic effect was negligible, i.e. the results of 2D analyses and the free field motion was almost the same. Besides, in the mesh sensitivity analyses for models, Kuhlemeyer and Lysmer (1973) criteria have been satisfied. Accordingly, all the mesh dimensions should be smaller than λ/10, in which λ is the shortest wavelength of the incident seismic motion.

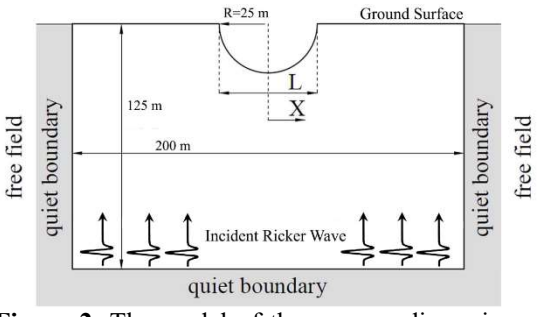

Figure 2. The model of the canyon, dimensions, applied boundary conditions, and Incident wave.

The accuracy and the feasibility of the numerical method for seismic analyses of topographic structures was verified through comparison of the numerical results with analytical solutions for the seismic response of a particular case of a semi-circular shaped canyon. Figure 2 shows the geometry, the dimension and the boundary condition of the modeled canyon. The canyon has the radius of R=25 m and the medium soil has the shear wave velocity of Vs=500 m/s, the Poisson's ratio of υ=1/3, and the mass density of ρ=2000 kg/m3. The canyon has been induced by the vertically propagating SV wave of Ricker type. Displacement equation of the Ricker wave is as follows:

$$f(t) = A_{max}\left[1 - 2\left(\pi.f_p(t-t_0)\right)^2\right].exp^{-(\pi.f_p(t-t_0))^2} \qquad (3)$$

where f_p, t_0, and A_{max} are the predominant frequency of Ricker wave, time shift parameter and the maximum amplitude of the displacement time history, respectively. The predominant frequency of the Ricker wave is 10 Hz, time shift parameter is 0.15 s and the maximum amplitude of the displacement time history is 1 mm that should result in maximum amplitude of 2 mm in the surface free field condition. Figure 3 shows the incident wave and free field motion time histories as well as the time domain seismic response of the selected points at the surface of the canyon. As can be seen, de-amplification of the motion in the center of the canyon is evident. Moreover, there is a clear amplification of the motion in the edge of the canyon.

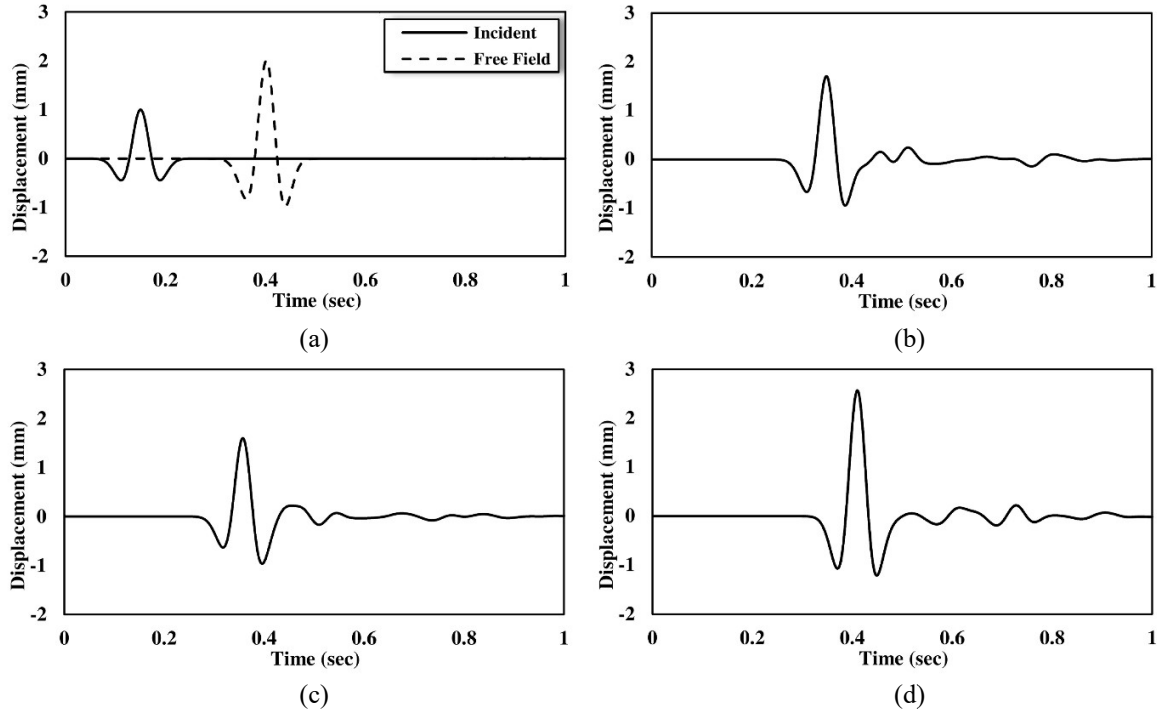

Figure 3. Time histories of (a) the incident and surface free field; the seismic response in (b) point x/R=0.0, (c) point x/R=0.5 and (d) point x/R=1.0 on the canyon.

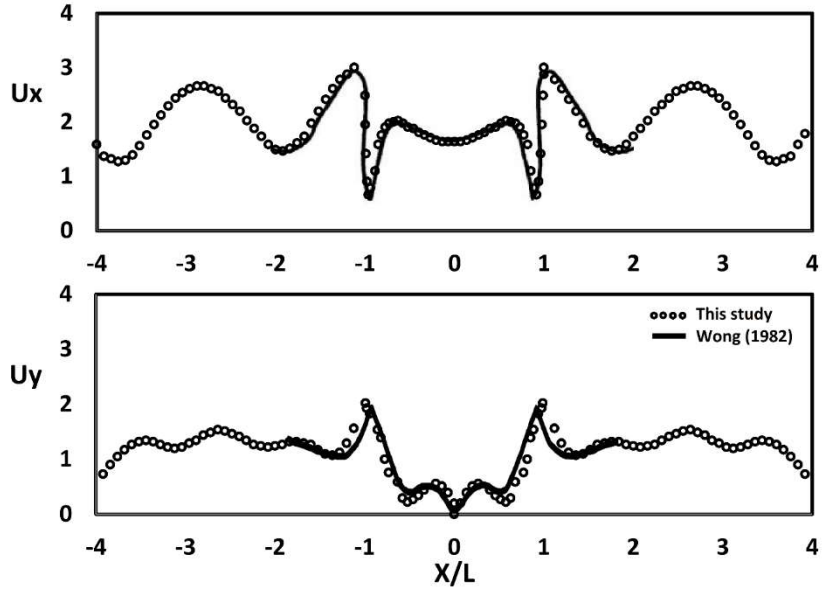

Figure 4. Numerical results for the canyon topography in comparison with analytical solution (Wong, 1982) in term of amplification with respect to the incident waves.

Wong (1982) used an analytical method to find the seismic response of a semi-circular shaped canyon for the particular wavelength of incident motions. For comparison, the Fourier transform of the time domain results have been performed and Fourier amplitude spectra have been calculated. Figure 4 shows the amplification values with respect to the incident motion for a particular wavelength ratio of λ/R=2 along with the analytical solution for the horizontal (Ux) and the vertical (Uy) components of the ground surface displacement.

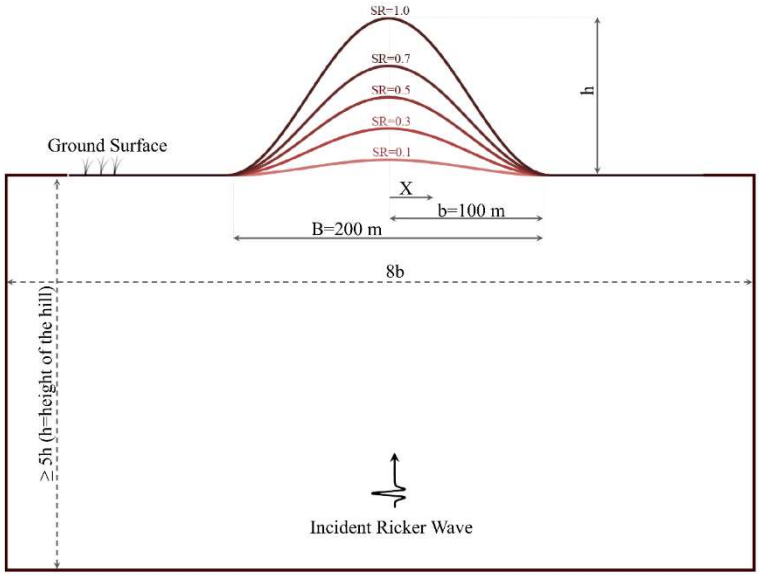

Figure 5. Geometrical parameters of the Gaussian-shaped hills as well as the model dimensions.

3 Methodology of Parametric Study

In order to investigate the amplification of time domain ground motion parameters by the topographic structures, the numerical seismic response of a set of the two-dimensional Gaussian-shaped hills has been studied. The geometry of the Gaussian-shaped hills is defined as follows:

$$\xi(x) = \begin{cases} 0.5h\left(1+\cos\left(\frac{\pi x}{b}\right)\right), & |x| \le b \\ 0, & |x| > b \end{cases} \quad (4)$$

where b and h denote the half-width and height of the hill, respectively. The Gaussian-shaped hills have the fixed half-width of 100 m and the different heights ranging from 10 m to 100 m. Figure 5 shows the geometry and dimensions of the modeled two-dimensional Gaussian-shaped hills. For simplicity, the shape ratio (SR), the ratio of height to half-width, is used as the geometrical factor of the studied hills. The shape ratios of considered hills are 0.1, 0.3, 0.5, 0.7, and 1.0. The medium is considered to be homogeneous linear elastic and has the shear wave velocity of 800 m/s (A-type soil condition of conventional building codes), the Poisson's ratio of υ=1/3, and the mass density of ρ=2400 kg/m^3. Considered models are impinged by the vertically propagating SV waves of Ricker type. To recognize the effects of the predominant frequency (or inversely the predominant period) of the incident motion on the time domain ground motion parameters, twelve incident Ricker waves with different periods have been applied. Displacement waveform of the Ricker wave presented in Equation (3). Velocity and acceleration waveform of the incident Ricker wave are as follows:

$$f'(t) = A_{max}.\begin{bmatrix} -4\pi^2.{f_p}^2(t-t_0).exp^{-\left(\pi.f_p(t-t_0)\right)^2} \\ -2\pi^2.{f_p}^2(t-t_0).\left(1-2\left(\pi.f_p(t-t_0)\right)^2\right).exp^{-(\pi.f_p(t-t_0))^2} \end{bmatrix} \quad (5)$$

$$f''(t) = A_{max}.\begin{bmatrix} -4\pi^2.{f_p}^2.exp^{-\left(\pi.f_p(t-t_0)\right)^2} + 16\pi^4.{f_p}^4(t-t_0)^2.exp^{-\left(\pi.f_p(t-t_0)\right)^2} \\ -2\pi^2.{f_p}^2.\left(1-2\pi^2.{f_p}^2(t-t_0)^2\right).exp^{-\left(\pi.f_p(t-t_0)\right)^2} \\ +4\pi^4.{f_p}^4\left(1-2\pi^2.{f_p}^2(t-t_0)^2\right).(t-t_0)^2.exp^{-\left(\pi.f_p(t-t_0)\right)^2} \end{bmatrix} \quad (6)$$

It is noteworthy that for simplicity all of the results have been discussed in the terms of dimensionless periods (T) defined as T=λ/2b; where λ is the wavelength and 2b is the hill width. In this way, twelve Ricker waves with displacement predominant dimensionless period of 0.2, 0.4, 0.6, 0.8, 1.0, 1.5, 2.0, 3.0, 4.0, 6.0, 8.0, and 10.0 have been used. The values of the maximum displacement amplitude for all the incident waves are the same and have been chosen to be 1 cm. The time shift parameters of the incident waves are proportional to the predominant period of the incident wave. It should be mentioned that in the case of the specific incident Ricker wave, the predominant frequency may differ for displacement, velocity, and acceleration. For example, in the case of the Ricker wave with displacement predominant period of 1.0, the velocity predominant period and the acceleration predominant period are √1.5 and √2, respectively.

Before the parametric analyses, the model dimension sensitivity analyses conducted in order to reduce the effects of artificial wave reflections from the boundaries at the areas of interest. It shows that by fixing the width of the hill as 200 m and variable height, the width and the height of the model should be set to 8b and 5h, respectively, which are generally compatible with those have been used by Bouckovalas and Papadimitriou (2005). Besides, the mesh dimension of the discretized area is properly chosen to fulfill the Kuhlemeyer and Lysmer criterion (1973) in which the effective element dimensions are less than λ/10; where λ is the wavelength of the considered wave.

4 Acceleration, Velocity, and Displacement Amplification Values

Based on the engineering interests, the general results obtained from the numerical analyses of the seismic responses of the two-dimensional Gaussian-shaped hills are presented. Figure 6 illustrates a part of time domain responses at selected points on the surface of the hills with different shape ratios. The selected points in each hill include the crest point, three points along the slope and the toe point of the hill. Incident waves are vertically propagating SV-waves of Ricker type with displacement predominant period of 1.0 sec and the time shift parameters of 2 sec. This means that the displacement predominant dimensionless period of 4.0, i.e. the predominant wavelength are four times the hills width. In three columns of Figure 6, the displacement, the velocity, and the acceleration time histories have been presented as well. The same scale has been used for presented plots for each component of the motion; where the general comparisons can be done easily. As can be seen, the motions have the highest values in the crest of the hills and from the crest points to the toe point amplitude of the all motion components (displacements, velocities, and accelerations) decrease. Figure 6 also shows the effects of the shape ratio in the time domain seismic response of the hills; as can be seen, the shape ratio or the geometry plays a remarkable role in controlling the seismic response of the hills. There is a little delay of wave arrival times related to the height of the selected points on the hills. Generally, in all of the selected points, the highest value of the motions belong to the highest hill and the amplitude of the motions decrease with decreasing shape ratio. Following the general pattern of the amplification along the hills, the effects of the shape ratio on seismic response decreases from crest points to the points along the slope of the hill and it can be ignored at the toe points.

The PGA, PGV, and PGD values of the surface motions at the selected points on the hills have been extracted and their

amplification with respect to the PGA, PGV, and PGD on the free field have been calculated. In Table 1, the results have been presented for five selected points on the hills, and the five shape ratios have been considered as well. Each row contains the amplification values for the specified dimensionless predominant period of the incident motions. A colored scale has been used for simplicity and trend evaluations, where the red colors express the amplification values and the blue colors express the de-amplification values, also the white color is set to the value of 1.0, i.e. the neutral value.

According to Table 1, it is evident that in most cases of the incident motions, the maximum amplification of motions has occurred on the crest of the hills. While, as another important result, it can be comprehended that the maximum de-amplifications in time domain do not necessarily occur at the hill-toe. This is in faint contrast to the common statement resulted from Figure 6, where only one specific dimensionless period of 4.0 has been taken into account. It is evident that the location of the occurrence of maximum de-amplification of motion in time domain varies with respect to the

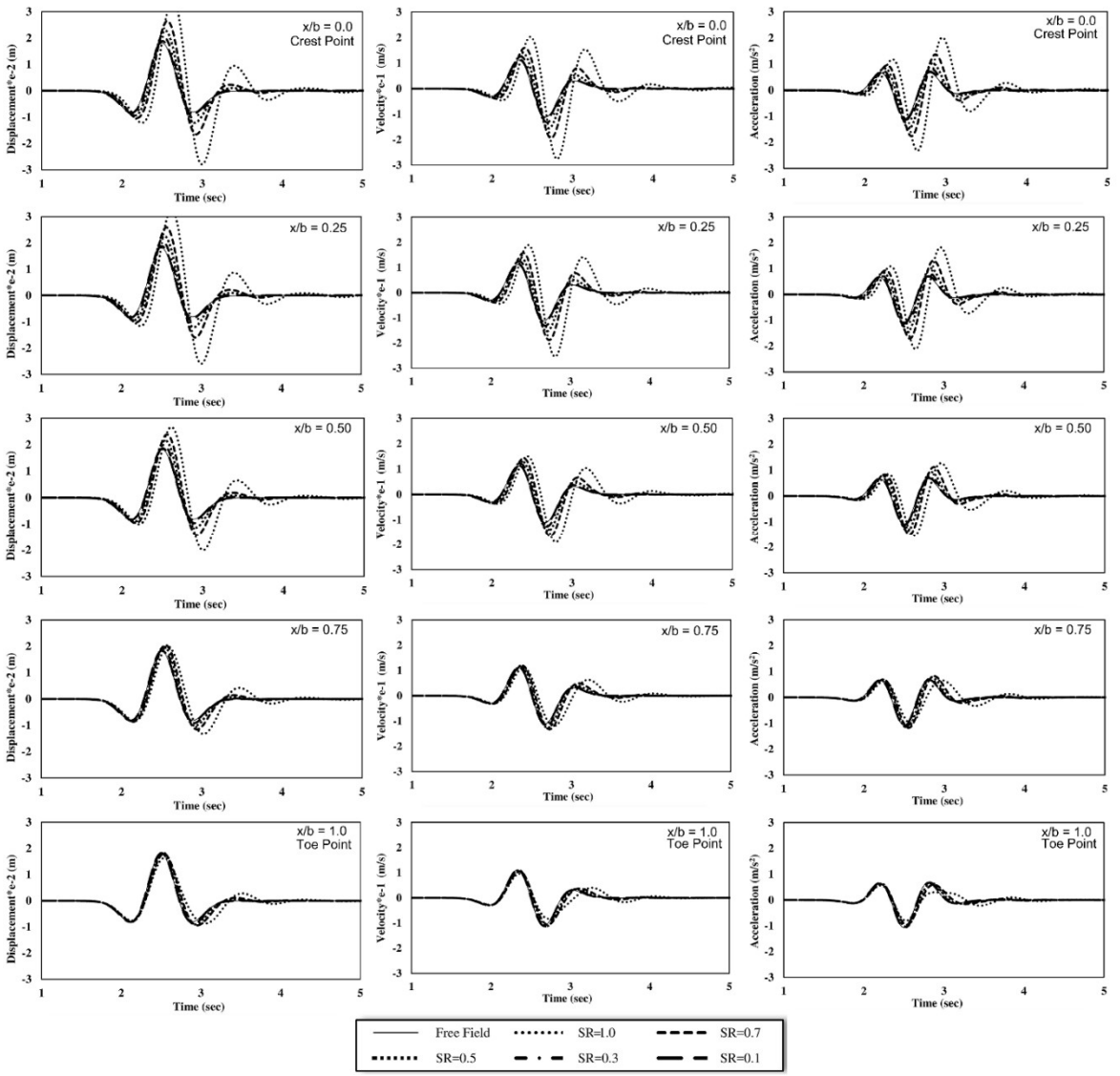

Figure 6. Time domain responses at five selected points on the hill surface against the Ricker SV waves with displacement predominant dimensionless period of 4.0.

Table 1. Amplification values of PGA, PGV and PGD for the Gaussian-Shaped Hills against the Ricker SV waves with different predominant periods.

Dimensionless Predominant Period		x/b = 0.0 (Crest Point) SR					x/b = 0.25 SR					x/b = 0.50 SR					x/b = 0.75 SR					x/b = 1.0 (Toe Point) SR				
		0.1	0.3	0.5	0.7	1.0	0.1	0.3	0.5	0.7	1.0	0.1	0.3	0.5	0.7	1.0	0.1	0.3	0.5	0.7	1.0	0.1	0.3	0.5	0.7	1.0
$T_{acc=}$	0.14	0.95	1.17	2.74	2.08	1.77	1.00	1.23	1.16	0.74	0.49	1.02	0.99	0.73	0.62	0.48	0.99	0.97	0.87	0.76	0.66	1.00	0.98	0.96	0.96	0.94
$T_{vel=}$	0.16	0.97	1.38	2.44	1.81	1.62	1.00	1.06	1.00	0.64	0.41	1.03	0.97	0.75	0.57	0.49	0.98	0.94	0.85	0.78	0.68	1.00	0.97	0.95	0.94	0.92
$T_{disp=}$	0.20	1.03	1.46	2.32	1.84	1.33	1.01	0.99	0.82	0.73	0.44	1.00	0.91	0.74	0.59	0.53	0.97	0.91	0.83	0.76	0.69	0.99	0.96	0.93	0.92	0.89
$T_{acc=}$	0.28	1.09	1.84	2.18	1.53	0.96	1.00	0.91	0.79	0.74	0.52	0.95	0.96	0.90	0.70	0.57	1.00	0.92	0.82	0.75	0.71	0.98	0.96	0.91	0.91	0.89
$T_{vel=}$	0.33	1.12	1.69	1.73	1.17	0.88	1.01	0.89	0.88	0.82	0.55	0.93	0.78	0.69	0.60	0.60	0.96	0.90	0.84	0.74	0.72	0.97	0.96	0.92	0.87	0.87
$T_{disp=}$	0.40	1.13	1.53	1.51	1.02	0.80	1.06	1.07	1.05	0.91	0.58	0.95	0.76	0.61	0.56	0.60	0.93	0.83	0.80	0.73	0.70	0.96	0.93	0.90	0.87	0.85
$T_{acc=}$	0.42	1.16	1.55	1.48	0.93	0.68	1.06	1.12	1.17	1.00	0.60	0.92	0.67	0.55	0.56	0.64	0.92	0.84	0.83	0.77	0.72	0.95	0.94	0.90	0.88	0.86
$T_{vel=}$	0.49	1.20	1.59	1.41	0.86	0.78	1.07	1.20	1.29	1.08	0.58	0.89	0.69	0.56	0.52	0.64	0.89	0.84	0.86	0.81	0.74	0.96	0.98	0.95	0.91	0.88
$T_{disp=}$	0.60	1.17	1.45	1.35	0.91	0.84	1.09	1.22	1.27	1.08	0.60	0.95	0.74	0.55	0.52	0.60	0.90	0.77	0.74	0.70	0.67	0.94	0.89	0.88	0.85	0.84
$T_{acc=}$	0.57	1.19	1.45	1.31	0.81	0.77	1.10	1.25	1.28	1.07	0.57	0.94	0.67	0.43	0.44	0.59	0.88	0.74	0.77	0.74	0.70	0.93	0.92	0.92	0.88	0.86
$T_{vel=}$	0.65	1.21	1.46	1.26	0.94	0.88	1.12	1.32	1.31	1.05	0.64	0.93	0.79	0.63	0.57	0.60	0.86	0.72	0.71	0.74	0.69	0.89	0.90	0.95	0.92	0.88
$T_{disp=}$	0.80	1.16	1.39	1.31	0.97	1.03	1.11	1.28	1.31	1.11	0.61	0.99	0.71	0.68	0.55	0.57	0.91	0.71	0.65	0.64	0.63	0.92	0.83	0.82	0.83	0.81
$T_{acc=}$	0.71	1.17	1.39	1.26	0.86	0.92	1.12	1.29	1.29	1.05	0.51	0.98	0.83	0.61	0.45	0.52	0.88	0.64	0.63	0.66	0.65	0.90	0.83	0.86	0.86	0.84
$T_{vel=}$	0.82	1.20	1.41	1.29	1.05	1.02	1.14	1.34	1.30	1.13	0.71	1.00	0.92	0.79	0.66	0.62	0.90	0.74	0.66	0.63	0.62	0.90	0.81	0.83	0.87	0.86
$T_{disp=}$	1.00	1.15	1.35	1.33	1.13	1.22	1.11	1.29	1.33	1.17	0.70	1.02	1.00	0.90	0.72	0.59	0.93	0.73	0.60	0.57	0.58	0.91	0.79	0.77	0.77	0.77
$T_{acc=}$	1.06	1.14	1.35	1.37	1.22	1.28	1.11	1.31	1.35	1.18	0.75	1.04	1.08	1.02	0.82	0.61	0.95	0.77	0.55	0.47	0.50	0.91	0.74	0.68	0.71	0.73
$T_{vel=}$	1.22	1.16	1.39	1.44	1.35	1.41	1.13	1.36	1.42	1.29	1.03	1.06	1.16	1.12	0.95	0.75	1.00	0.87	0.72	0.64	0.61	0.94	0.82	0.75	0.74	0.74
$T_{disp=}$	1.50	1.11	1.30	1.41	1.44	1.60	1.09	1.28	1.39	1.38	1.20	1.04	1.13	1.15	1.04	0.75	0.98	0.91	0.76	0.63	0.57	0.95	0.82	0.72	0.69	0.69
$T_{acc=}$	1.41	1.12	1.32	1.45	1.49	1.61	1.10	1.29	1.42	1.40	1.19	1.05	1.15	1.18	1.04	0.68	0.99	0.93	0.77	0.61	0.55	0.95	0.82	0.68	0.64	0.65
$T_{vel=}$	1.63	1.13	1.36	1.56	1.69	1.85	1.11	1.34	1.53	1.57	1.44	1.06	1.21	1.29	1.15	0.89	1.02	0.99	0.87	0.77	0.69	0.97	0.89	0.80	0.74	0.72
$T_{disp=}$	2.00	1.09	1.26	1.43	1.59	1.86	1.08	1.24	1.41	1.52	1.55	1.05	1.15	1.24	1.22	0.95	1.01	1.01	0.94	0.83	0.69	0.98	0.91	0.80	0.73	0.69
$T_{acc=}$	2.12	1.18	1.25	1.46	1.70	2.05	1.07	1.23	1.43	1.62	1.77	1.05	1.16	1.29	1.33	1.08	1.01	1.04	1.02	0.92	0.70	0.99	0.95	0.86	0.74	0.69
$T_{vel=}$	2.45	1.08	1.27	1.53	1.88	2.40	1.07	1.25	1.51	1.80	2.12	1.05	1.19	1.36	1.49	1.33	1.02	1.07	1.09	1.03	0.85	1.00	0.97	0.92	0.85	0.79
$T_{disp=}$	3.00	1.06	1.18	1.35	1.58	2.02	1.05	1.17	1.34	1.54	1.83	1.04	1.13	1.24	1.34	1.34	1.02	1.05	1.07	1.06	0.91	1.00	0.99	0.95	0.88	0.79
$T_{acc=}$	2.83	1.16	1.18	1.37	1.64	2.16	1.05	1.17	1.35	1.59	1.98	1.04	1.13	1.26	1.40	1.44	1.02	1.06	1.09	1.10	0.92	1.00	1.00	0.97	0.89	0.75
$T_{vel=}$	3.27	1.05	1.19	1.40	1.74	2.48	1.05	1.18	1.38	1.69	2.29	1.04	1.14	1.30	1.50	1.72	1.02	1.08	1.14	1.20	1.08	1.01	1.02	1.01	0.96	0.87
$T_{disp=}$	4.00	1.04	1.13	1.26	1.46	1.92	1.04	1.12	1.25	1.43	1.81	1.03	1.10	1.20	1.32	1.47	1.02	1.05	1.09	1.13	1.10	1.01	1.02	1.01	0.99	0.90
$T_{acc=}$	4.24	1.03	1.11	1.23	1.42	1.92	1.03	1.11	1.22	1.40	1.83	1.02	1.09	1.18	1.31	1.56	1.02	1.06	1.10	1.16	1.22	1.01	1.03	1.04	1.05	1.00
$T_{vel=}$	4.90	1.03	1.11	1.23	1.44	2.04	1.03	1.11	1.23	1.42	1.95	1.03	1.09	1.19	1.34	1.68	1.02	1.06	1.12	1.20	1.34	1.01	1.04	1.07	1.09	1.10
$T_{disp=}$	6.00	1.02	1.07	1.15	1.26	1.57	1.02	1.07	1.14	1.25	1.53	1.02	1.06	1.12	1.20	1.38	1.01	1.04	1.07	1.12	1.18	1.01	1.02	1.04	1.05	1.05
$T_{acc=}$	5.66	1.02	1.07	1.14	1.26	1.58	1.02	1.07	1.14	1.24	1.53	1.02	1.06	1.12	1.20	1.39	1.01	1.04	1.08	1.12	1.21	1.01	1.02	1.04	1.06	1.08
$T_{vel=}$	6.53	1.02	1.07	1.13	1.24	1.56	1.02	1.06	1.13	1.23	1.52	1.02	1.05	1.11	1.19	1.40	1.01	1.04	1.08	1.13	1.24	1.01	1.03	1.05	1.07	1.12
$T_{disp=}$	8.00	1.01	1.04	1.09	1.15	1.33	1.01	1.04	1.08	1.14	1.30	1.01	1.04	1.07	1.12	1.23	1.01	1.03	1.05	1.08	1.13	1.00	1.02	1.03	1.04	1.06
$T_{acc=}$	7.07	1.01	1.05	1.09	1.16	1.35	1.01	1.04	1.09	1.15	1.32	1.01	1.04	1.08	1.13	1.25	1.01	1.03	1.05	1.08	1.15	1.01	1.02	1.03	1.04	1.07
$T_{vel=}$	8.17	1.01	1.04	1.08	1.14	1.31	1.01	1.04	1.08	1.13	1.29	1.01	1.03	1.07	1.11	1.22	1.01	1.03	1.05	1.08	1.14	1.01	1.02	1.03	1.05	1.07
$T_{disp=}$	10.00	1.01	1.03	1.05	1.09	1.19	1.01	1.03	1.05	1.09	1.18	1.01	1.02	1.04	1.07	1.14	1.00	1.02	1.03	1.05	1.08	1.00	1.01	1.02	1.03	1.04

dimensionless periods of the incident motions. Roughly speaking, as the dimensionless period of the incident motions decreases; in each case of displacement, velocity, or acceleration; the location of the minimum amplification, or de-amplification, on the surface moves upside the hill.

A close examination of Table 1 leads us to conclude that the seismic response of the hills is generally amplified when impinged by the incident waves with very long wavelengths, i.e. displacement predominant dimensionless period equal or greater than 6.0. In these cases of incident motions, the maximum amplification values of the motion increase with the shape ratio. For middle wavelengths, i.e. displacement predominant dimensionless period of greater than 1.0 to 4.0, the most part of the hills would experience the amplification, but in some parts of the hill in the toe side, de-amplifications will occur. In these cases of incident motions, generally, the amplifications on crest side and de-amplification on the toe side of the hills increases with increasing shape ratios. For short wavelength, i.e. incident motions with a predominant wavelength

less than the hill width, de-amplifications on the hills, especially on the toe side, are predominant, where its maximum location moves upward on the hill with decreasing wavelength. In the later cases of the incident motion, amplifications only could be seen on the crest point and the point near the crest of the hills. In these cases, the maximum amplifications or de-amplifications do not belong to the maximum shape ratio, i.e. the highest hill, and the maximum values have been occurred in the middle shape ratios.

Additionally, presented amplification values in the table reveal that, for a specific point on a hill with a specific shape ratio and almost the same predominant dimensionless period for incident motion (regardless of its motion type i.e. displacement, velocity or acceleration), there is a comparable amplification value. This similarity of amplification for a particular predominant dimensionless period could be followed in different shape ratios.

5 Time Domain Amplifications against Fourier Amplifications

It is common to state the site effects on the ground motion during earthquakes by using the Fourier amplification curves. Such amplification curves for each point could be calculated using the ratio of the Fourier amplitude of the motion with respect to the Fourier amplitude of the reference motion at the desired reference point. For a linear elastic system and a given frequency of the input motion, the seismic response amplification with respect to the input motion is independent of the amplitude of the input. For this type of system, i.e. those considered in this study, unique Fourier amplification curves are expected for each observation points, regardless of the input motion amplitudes. At the current study, the Fourier amplification curves of the motion have been calculated for the selected points on the hills with respect to the free field motions. As expected for any given point on the hill, the Fourier amplification curves in the cases of various predominant periods of incident motions were completely compatible with each other. The representative Fourier amplification curves for each point, compiled from the twelve Fourier amplification curves for twelve predominant periods of the input motions, have been presented in Figure 7. In this figure, also the amplification of PGA, PGV, and PGD values have been presented against the predominant dimensionless period of their input motions. Calculations of Fourier amplification curves and extraction of peak ground motions had been done for all shape ratios and the graphs were provided for five shape ratios; however, considering that the amplification values in shape ratio of 0.1 for both time domain and frequency domain are ignorable, its results are not presented in Figure 7.

As can be seen, the seismic responses of the two-dimensional Gaussian-shaped hills consist of the amplification and the de-amplification, with regard to the frequency content of the input motion. This behavior can be comprehended from both time domain amplification ratios of PGA, PGV, and PGD values as well as the Fourier amplification ratios. There is a gentle variation of the Fourier amplification curves in the crest and the crest side of the hills; while there is a large variation of the Fourier amplification curves in the toe and the toe side of the hills. Increasing the shape ratio of the hill intensifies the severity of the Fourier amplification curve with a dimensionless period. In contrast, the time domain amplifications of PGA, PGV, and PGD values generally have a gentle variation with the dimensionless predominant period in all points of observation and shape ratios. This is not surprising, where the time domain amplification values contain the seismic

responses over a range of a frequency content of the input motion, i.e. the same as a weighted average of the seismic response around the given predominant period. Taking the later mentioned issue and Figure 7 into account, it can be seen that there are general agreements between the results of the time domain amplification of PGA, PGV, and PGD values and that of the frequency domain, the Fourier amplification ratios. Precisely speaking, there are characteristic dimensionless periods, more than ~1.0 in all shape ratios, at which a well-matched relationship can be observed between both groups of time domain and frequency domain amplifications. For the dimensionless period range less than ~1.0, time domain results seem to show a

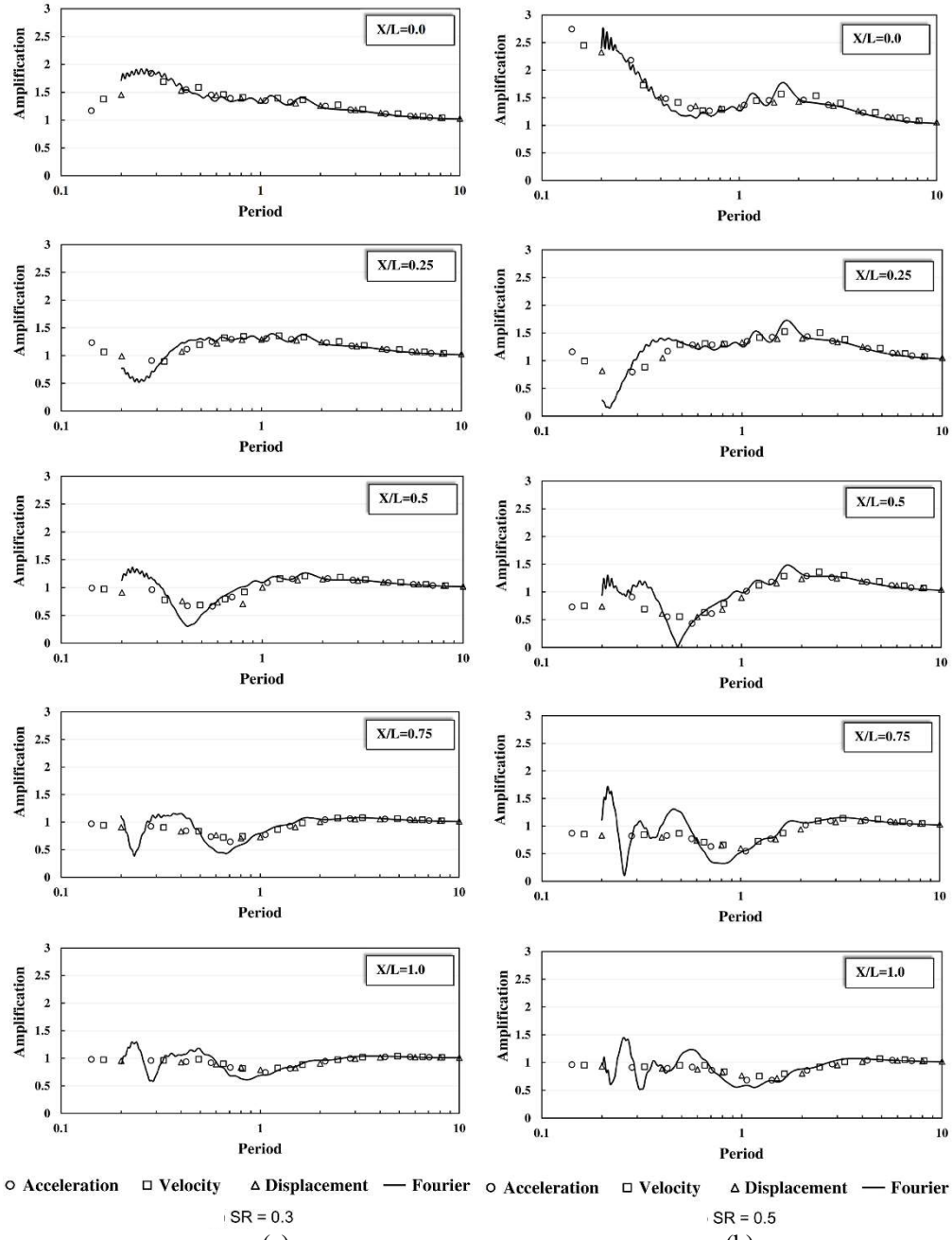

Figure 7. Fourier amplification ratio vs. dimensionless period along with amplification of PGA, PGV, PGD.

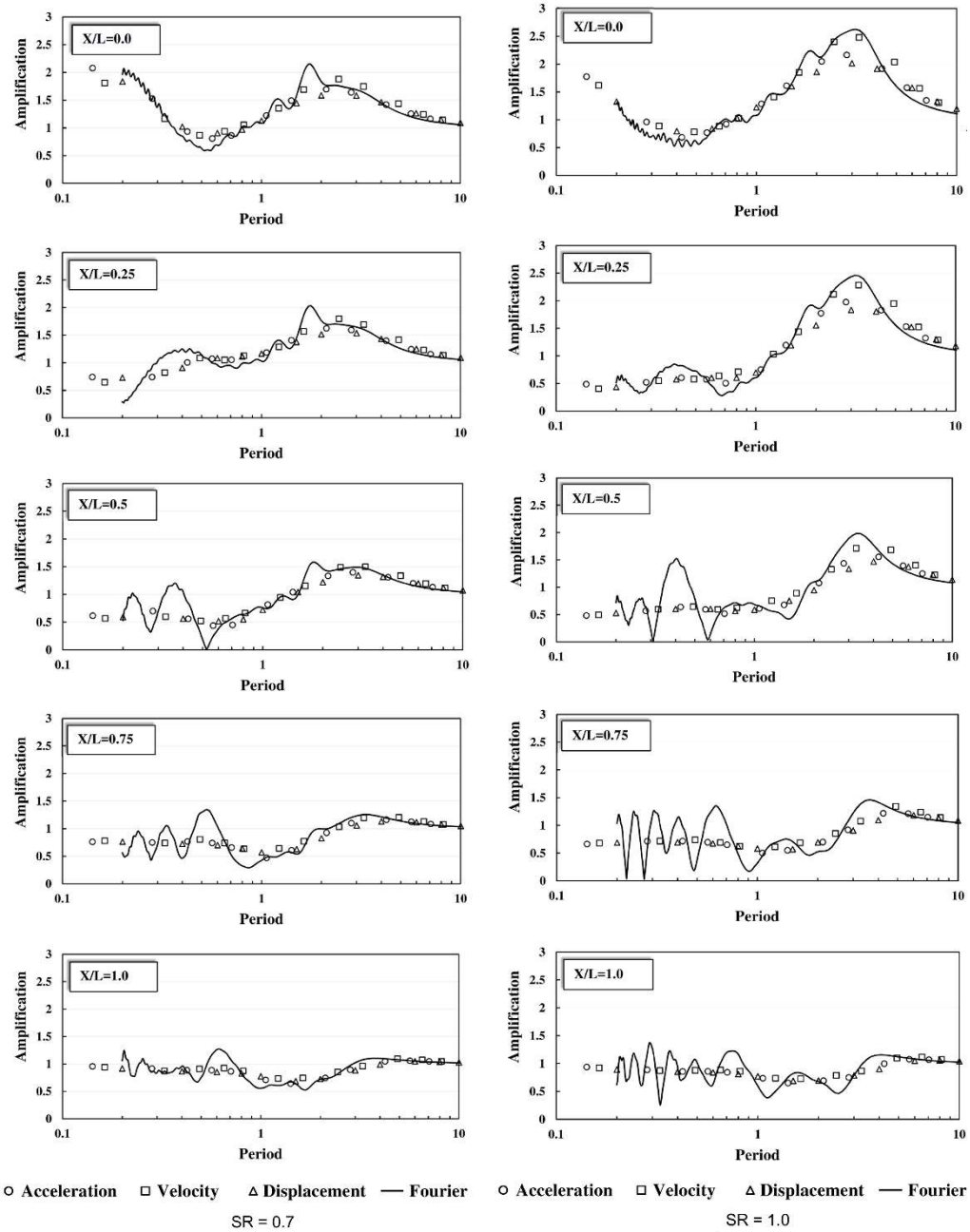

Figure 7 continue.

regular behavior, but frequency amplification curves are fluctuated drastically, that made it hard to conclude in a detailed manner; however, there is a general agreement yet, if the averaged Fourier amplification would be considered. As another fact, it can be seen that in almost any case, the amplification values, whether in the time domain (amplification of the peak acceleration, velocity, and displacement) or in the frequency domain (the Fourier amplification ratios), gradually reach to 1.0 at dimensionless period 10. It means that it is unlikely to have amplification or de-amplification potential for a dimensionless period more than 10, i.e. waves with the wavelength greater than 10 time the hill width.

When two groups of time domain and frequency domain results are compared against dimensionless period, it can be

concluded that one can use amplification ratios in the frequency domain to estimate the amplification ratios in the time domain at any point along the hill. This is more reliable if the averaged Fourier amplifications over a frequency range would be used instead of the explicit Fourier amplification curves. Subsequently, this issue paves the way to use results of previous studies, most of which were conducted in the frequency domain, to evaluate the amplification potentials of PGA, PGV, and PGD in the time domain.

6 Conclusion

The clear perspectives of the amplification of peak ground acceleration, velocity, and displacement of two-dimensional Gaussian-shaped hills subjected to vertically propagating SV Ricker wave were presented. Presented results show that the response of the hill against the large wavelength (greater than the six times the hill width) is totally amplification, the quantity of which related to the point location on the hill and the height of the hill. In middle wavelength (equal to hill width to less than four times the hill width) seismic response is amplified in crest side and is de-amplified in toe side, where amplifications or de-amplifications is increased with hill height. For short wavelengths (less than the hill width), the seismic response on the most part of the hill is de-amplified and amplification exists only on the crest and near crest points, where the maximum amplification or de-amplifications do not necessarily belong to the high hills. Generally, by decreasing the predominant period of the incident motions, the de-amplification zones have been developed on the hill and location of the maximum de-amplification values moves upside the hill. Comparison of the amplification of PGA, PGV, and PGD values with the common Fourier amplification curves showed that, in general, there is a well-matched correlation; meanwhile, the time domain amplifications of PGA, PGV, and PGD values have a gentle variation with the dimensionless predominant period. It seems that one can give a reliable estimate of time domain amplification of PGA, PGV, and PGD using averaged Fourier amplifications over the suitable range of frequency around the predominant period of input motion.

Acknowledgement

The authors would like to thank the anonymous reviewers for their careful reading of the manuscript and their many insightful comments and suggestions that greatly improved the paper.

References

Ashford, S. A., Sitar, N., Lysmer, J., and Deng, N., 1997, Topographic effects on the seismic response of steep slopes: Bulletin of the Seismological Society of America, **87**(3), 701-709.

Athanasopoulos, G., Pelekis, P., and Leonidou, E., 1999, Effects of surface topography on seismic ground response in the Egion (Greece) 15 June 1995 earthquak: Soil Dynamics and Earthquake Engineering, **18**(2), 135-149.

Bard, P. Y., 1982, Diffracted waves and displacement field over two-dimensional elevated topographies: Geophysical Journal of the Royal Astronomical Society, **71**(3), 731-760.

Boore, D. M., 1972, A note on the effect of simple topography on seismic SH waves: Bulletin of the Seismological Society of America, **62**(1), 275-284.

Boore, D. M., 1973, The effect of simple topography on seismic waves: Implications for the accelerations recorded at Pacoima dam, San Fernando Valley, California: Bulletin of the Seismological Society of America, **63**(5), 1603-1609.

Bouchon, M., 1973, Effect of topography on surface motion: Bulletin of the Seismological Society of America, **63**(2), 615-632.

Bouckovalas, G. D., and Kouretzis, G., 2001, Stiff soil amplification effects in the 7 September 1999 Athens (Greece) earthquake: Soil Dynamics and Earthquake Engineering, **21**(8), 671-687.

Bouckovalas, G. D., and Papadimitriou, A. G., 2005, Numerical evaluation of slope topography effects on seismic ground motion: Soil Dynamics and Earthquake Engineering, **25**(7), 547-558.

Building Standard Law of Japan (BSL), 2004, Building Research Institute, Tokyo, Japan.

Celebi, M., 1991, Topographical and geological amplification, case studies and engineering implications: Structural Safety, **10**(1), 199-217.

Celebi, M., 1987, Topographical and geological amplifications determined from strong-motion and aftershock records of the 3 March 1985 Chile earthquake: Bulletin of the Seismological Society of America, **77**(4), 1147-1167.

ITASCA, 2017, FLAC 3D (Fast Lagrangian Analysis of Continua): Itasca Consulting Group Inc., Minneapolis, Minnesota, USA.

Kamalian, M., Gatmiri, B., and Sohrabi-Bidar, A., 2003, On time-domain two-dimensional site response analysis of topographic structures by BEM: Journal of Seismology and Earthquake Engineering, **5**(2), 35-45.

Kamalian, M., Jafari, M., Sohrabi-Bidar, A., Razmkhah, A., and Gatmiri, B., 2006, Time-domain two-dimensional site response analysis of non-homogeneous topographic structures by a hybrid BE/FE method: Soil Dynamics and Earthquake Engineering, **26**(8), 753-765.

Kamalian, M., Sohrabi-Bidar, A., Razmkhah, A., Taghavi, A., and Rahmani, I., 2008, Considerations on seismic micro zonation in areas with two-dimensional hills: Journal of Earth System Science, **117**(2), 783-796.

Kuhlemeyer, R. L., Lysmer, J., 1973, Finite element method accuracy for wave propagation problems: Journal of the Soil Mechanics and Foundations Division, **99** (Tech Rpt.).

Sánchez-Sesma, F. J., and Campillo, M., 1991, Diffraction of P, SV, and Rayleigh waves by topographic features: A boundary integral formulation: Bulletin of the Seismological Society of America, **81**(6), 2234-2253.

Sánchez-Sesma, F. J., and Campillo, M., 1993, Topographic effects for incident P, SV and Rayleigh waves. Tectonophysics, **218**(1), 113-125.

Sohrabi-Bidar, A., Kamalian, M., and Jafari, M., 2009a, Seismic waves scattering in three-dimensional homogeneous media using time-domain boundary element method: Journal of the Earth and Space Physics.

Sohrabi-Bidar, A., Kamalian, M., and Jafari, M., 2009b, Time-domain BEM for three-dimensional site response analysis of topographic structures: International Journal for Numerical Methods in Engineering, **79**(12), 1467-1492.

Sohrabi-Bidar, A., Kamalian, M., and Jafari, M., 2010, Seismic response of 3-D Gaussian-shaped valleys to vertically propagating incident waves: Geophysical Journal International, **183**(3), 1429-1442.

Solomos, G., Pinto, A., and Dimova, S., 2008, A review of the seismic hazard zonation in national building codes in the context of Eurocode 8, Support to the Implementation, Harmonization and Further Development of the Eurocodes: Italy, JRC European Commission; **3**.

Spudich, P., Hellweg, M., and Lee, W., 1996, Directional topographic site response at tarzana observed in aftershocks of the 1994 Northridge, California, earthquake: implications for main-shock motions: Bulletin of the Seismological Society of America, **86**(1B), S193-S208.

Trifunac, M. D., and Hudson, D. E., 1971, Analysis of the Pacoima dam accelerogram San-Fernando, California, earthquake of 1971: Bulletin of the Seismological Society of America, **61**(5), 1393-1411.

Wang, F., Miyajima, M., Dahal, R., Timilsina, M., Li, T., Fujiu, M., Kuwada, Y., and Zhao, Q., 2016, Effects of topographic and geological features on building damage caused by 2015.4. 25 Mw 7.8 Gorkha earthquake in Nepal, a preliminary investigation report: Geoenvironmental Disasters, **3**(1), 1-17.

Wong, H., 1982, Effect of surface topography on the diffraction of P, SV, and Rayleigh waves: Bulletin of the Seismological Society of America, **72**(4), 1167-1183.

Zhang, B., Papageorgiou, A. S., and Tassoulas, J. L., 1998, A hybrid numerical technique, combining the finite-element and boundary-element methods, for modeling the 3D response of 2D scatterers: Bulletin of the Seismological Society of America, **88**(4), 1036-1050.